850-59

AMERICAN ROCKET SOCIETY

ARS

A national association for the advancement of rocketry, jet propulsion and astronautics

500 FIFTH AVENUE • NEW YORK 36, N. Y.

MEASUREMENTS OF HEAT-TRANSFER AND FRICTION COEFFICIENTS FOR HELIUM FLOWING IN A TUBE AT SURFACE TEMPERATURES UP TO 5900°R

by

Maynard F. Taylor and Thomas A. Kirchgessner
Lewis Research Center
National Aeronautics and Space Administration

Presented at the ARS Semi-Annual Meeting, June 8-11, 1959, San Diego, California.

850-59

TMX#

MCN 2/8/66

MEASUREMENTS OF HEAT-TRANSFER AND FRICTION COEFFICIENTS FOR HELIUM FLOWING IN A TUBE AT SURFACE TEMPERATURES UP TO 5900° R

By Maynard F. Taylor and Thomas A. Kirchgessner

Lewis Research Center
National Aeronautics and Space Administration
Cleveland, Ohio

E-474

SUMMARY

Measurements of average heat-transfer and friction coefficients and local heat-transfer coefficients were made with helium flowing through electrically heated smooth tubes with length-to-diameter ratios of 60 and 92 for the following range of conditions: average surface temperature from 1457° to 4533° R, Reynolds number from 3230 to 60,000, heat flux up to 345,000 Btu per hour per square foot of heat transfer area, and exit Mach number to 1.0.

The results indicate that in the turbulent range of Reynolds number based on tube diameter, good correlation of the local heat-transfer coefficients is obtained when the physical properties and density of helium are evaluated at a reference film temperature midway between the surface and fluid bulk temperature. The average heat-transfer coefficients are best correlated on the basis that the coefficient varies with $\left[1 + \left(\frac{L}{D}\right)^{-0.7}\right]$ and the physical properties and density are evaluated at the surface temperature. The average friction coefficients for the tests with no heat addition are in complete agreement with the Karman-Nikuradse line. The average friction coefficients for the case of heat addition are in poor agreement with the accepted line.

INTRODUCTION

The importance of nuclear reactors as a power source for aircraft and space vehicles has stimulated interest in convective heat transfer from high-temperature surfaces. The resulting large ratio of fuel element temperature to working fluid temperature means a large variation in the properties of the fluid, which influence the heat-transfer characteristics. Some work has been done with wall temperatures up to 3460° R using air (ref. 1). Heat-transfer coefficients for helium flowing through a carbon tube with a maximum inside surface temperature of 5040° R and a corresponding gas temperature of 4640° R are presented in Ref. 2.

In order to extend the range of surface temperature reported in Ref. 1 and the ratio of surface-to-fluid bulk temperature of Ref. 2, the experimental apparatus for the present investigation was set up at the NASA Lewis Research Center. In this investigation the wall temperatures were increased to the limit of the tungsten and molybdenum test sections while the ratio of surface-to-fluid bulk temperature was kept as high as possible.

SYMBOLS

A	cross-sectional area of tube wall, ft
C_1	constant
C_2	constant, 25,891 micron °R
c_p	specific heat of helium at constant pressure, Btu/(lb)(°R)
D	inside diameter of test section, ft
E	voltage drop across test section, v
e	voltage drop across an increment of test section, v
f	average friction coefficient

G	mass flow per unit cross-sectional area, lb/(hr)(sq ft)
g	acceleration due to gravity, 4.17×10^8 ft/hr^2
h_{av}	average heat-transfer coefficient, Btu/(hr)(sq ft)($^\circ$R)
h	local heat-transfer coefficient, Btu/(hr)(sq ft)($^\circ$R)
I	current flow through test section, amp
J_{bb}	rate of emission of radiant energy per unit area per wavelength from blackbody, Btu/(hr)(sq ft)(micron)
J_{br}	rate of emission of radiant energy per unit area per wavelength from nonblackbody, Btu/(hr)(sq ft)(micron)
J_τ	rate of transmission through view window of radiant energy per unit area per wavelength from nonblackbody, Btu/(hr)(sq ft)(micron)
k	thermal conductivity of helium, Btu/(hr)(sq ft)($^\circ$R/ft)
k_t	thermal conductivity of test section material, Btu/(hr)(sq ft)($^\circ$R/ft)
k_z	thermal conductivity of insulating material, Btu/(hr)(sq ft)($^\circ$R/ft)
ΔL	incremental heat-transfer length, ft
L	heat-transfer length of test section, ft
Nu	Nusselt number based on local heat-transfer coefficient, hD/k
Nu_{av}	Nusselt number based on average heat-transfer coefficient, $h_{av}D/k$
P	absolute total pressure, lb/sq ft
p	absolute static pressure, lb/sq ft
Δp	over-all static-pressure drop across test section, lb/sq ft
Δp_{fr}	friction static-pressure drop across test section, lb/sq ft
Δp_{mom}	momentum static-pressure drop across test section, lb/sq ft
Q	rate of heat transfer to gas, Btu/hr
Q_E	rate of electrical heat input to test section, Btu/hr

Q_e	rate of electrical heat input to increment, Btu/hr
Q_c	rate of heat conduction through tube wall in the axial direction, Btu/hr
Q_L	rate of heat loss to the surroundings, Btu/hr
$Q_{\Delta L}$	rate of heat loss radially to the surroundings from an increment, Btu/hr
R	gas constant for helium, 386 (ft)(lb)/(lb)(^oR)
r_i	inside radius of insulating cylinder, ft
r_o	outside radius of insulating cylinder, ft
S	heat-transfer area of test section, sq ft
T	total or stagnation temperature, ^oR
T_b	average bulk temperature, $(T_1 + T_2)/2$, ^oR
T_{bb}	blackbody temperature, ^oR
T_{br}	brightness temperature (apparent temperature of nonblackbody), ^oR
T_f	average film temperature, $(T_s + T_b)/2$, ^oR
T_s	average inside surface temperature of test section, ^oR
T_τ	apparent brightness temperature (apparent temperature of nonblackbody with view window interposed), ^oR
T_{zi}	temperature of inner wall of insulating cylinder, ^oR
T_{zo}	temperature of outer wall of insulating cylinder, ^oR
t	static temperature, ^oR
V	bulk velocity of gas, ft/hr
W	helium flow, lb/hr
x	distance from entrance of test section, ft
γ	ratio of specific heats of helium
ϵ_λ	spectral emissivity

λ wavelength (effective wavelength of small target optical pyrometer filter), micron

μ absolute viscosity of helium, lb/(hr)(ft)

ρ density of helium, lb/cu ft

ρ_{av} average density of helium defined by $(p_1 + p_2)/R(t_1 + t_2)$, lb/cu ft

τ_λ spectral transmissivity of view window

$\frac{c_p \mu}{k}$ Prandtl number

$\frac{\rho V D}{\mu}$ Reynolds number

$\frac{hD}{k}$ Nusselt number

Subscripts:

b bulk (when applied to properties, indicates evaluation at average bulk temperature, T_b)

f film (when applied to properties, indicates evaluation at average film temperature, T_f)

s surface (when applied to properties, indicates evaluation at average surface temperature, T_s)

1 test section entrance

2 test section exit

EXPERIMENTAL APPARATUS

Arrangement

A schematic diagram of the arrangement of the test section and equipment used in the investigation is shown in Fig. 1. Dry helium, contained in a pressurized tank, was passed through the pressure-regulating valve into a rotometer and then to a mixing tank, which consisted of three

concentric passages with baffles in the center passage. After mixing, the gas passed through the electrically heated test section into a second mixing tank of a design similar to the first tank and then exhausted into the atmosphere. The molybdenum test section was thermally insulated with a molybdenum radiation shield surrounded with zirconium oxide insulating grains. The zirconium oxide grains were held in place by a surrounding transite cylinder. The tungsten test section was insulated only with a radiation shield. The mixing tanks, test section, and transite cylinder were housed in a vacuum-tight steel containment tank, which was evacuated to about 50 microns of mercury. This was done to minimize oxidation of the refractory materials used as test sections. Pressures lower than 50 microns of mercury were possible but would have resulted in evaporation of the hot metals. Figure 2 shows a photograph of the setup with the containment tank removed.

Electric power was supplied to the test section through water-cooled copper tubing from a 208-volt 60-cycle supply line through a 100-kva power transformer and a 125-volt DC saturable core reactor. The saturable core reactor permitted voltage regulation from approximately 3 to 25 volts. A voltmeter was used directly to read the potential across the complete test section and across seven incremental lengths of the test section. Current was read on an ammeter used with an 800 to 1 current transformer.

Test Sections

Since the object of this investigation was to obtain heat-transfer data at as high a surface temperature as possible, this experiment embraced a number of materials problems. There are only five known metals with melting points above 4500° F: molybdenum, osmium, tantalum, rhenium, and

tungsten in the order of increasing melting points. All five of these materials are subject to rapid oxidation when heated in air. For reasons of availability and high melting point, molybdenum and tungsten were chosen as test section material. Molybdenum tubes were available commercially so they were used for the first tests. Several tubes were made by disintegrating holes through tungsten rods, which were then ground to a uniform wall thickness. Nickel entrance and molybdenum exit flanges were used to connect the test sections to the mixing tanks. A shrink fit combined with very careful welding was found to be a satisfactory method of attaching the flanges to the test section. The molybdenum test section was equipped with a bellmouth entrance. A right-angle edge approach was used for the tungsten test section entrance.

The dimensions of the various tubes used as test sections in this investigation are shown below:

Tube material	Inside diameter, in.	Outside diameter, in.	H.T. length, in.	L/D
Molybdenum	0.191	0.250	11.5	60
Tungsten	.125	.250	11.5	92

Instrumentation

The outside wall temperatures of the test section were measured with 24-gauge platinum - platinum - 13 percent rhodium thermocouples spot welded along the length, located as shown in Fig. 3. For test section temperatures beyond the range of the thermocouples, a small target optical pyrometer was used. The use of the optical pyrometer is discussed in the appendix. Some experimentation with tungsten-molybdenum thermocouples

was conducted but the extreme brittleness of the tungsten wire after welding made the use of this thermocouple impractical.

The gas temperature was measured before entering and after leaving the test section with platinum - platinum-rhodium thermocouples located downstream of the baffles in the two mixing tanks.

The radiation shield and outside surface of the transite insulating cylinder were instrumented with platinum - platinum-rhodium thermocouples. Molybdenum wire was spot welded along the test section to measure voltage drop as a function of distance from the entrance. Locations are shown in Fig. 3. Static-pressure taps were located in the entrance mixing tank, and in the entrance and exit flanges of the molybdenum test section, as shown in Fig. 3. The flanges of the tungsten test section were not instrumented with pressure taps because of the difficulty in getting holes through the walls of the tungsten tube.

TEST PROCEDURE

The following procedure was used in obtaining adiabatic friction data: the helium flow rate was set to a desired value and when steady-state conditions were attained, the flow rate, pressure readings, and inlet gas temperature were recorded. The helium flow rate was then set to a higher value and when steady-state conditions were attained, the experimental data were again recorded. The process was repeated until the available flow rate range had been covered.

Heat-transfer and friction data for the heated test runs were obtained by the following general procedure: After the helium flow rate had been set to the desired value, the electric power across the test section was adjusted to give the desired test section temperature. When

steady-state conditions were attained, the flow rate, electrical power input, pressures, and temperatures were recorded. The helium flow rate and electrical power input were then set to higher values, and the process repeated until the available Reynolds number range and test section temperature range had been covered.

The molybdenum test section was used in obtaining both heat-transfer and friction factor data. Since the tungsten test section was not instrumented with pressure taps, it was used only in obtaining heat-transfer data.

The range of conditions for which data were obtained is summarized in the following table:

Test section material	Bulk Reynolds number range	Average surface temperature range, ^{o}R	Exit Mach number range	Heat flux range, Btu/(hr)(sq ft)
Molybdenum	3,750 to 60,000	530	0.09 to 0.97	Adiabatic
Molybdenum	3,230 to 25,230	1457 to 2334	0.21 to 0.95	71,000 to 290,000
Tungsten	5,375 to 11,000	1905 to 4533	0.72 to 1.0	155,000 to 345,000

METHOD OF CALCULATION

Helium Properties

The variable physical properties of helium used in calculating the Nusselt, Reynolds, and Prandtl numbers are shown in figure 4 as a function of temperature. In the absence of experimental data, the curves in figure 4 were calculated by the methods shown in references 3, 4, and 5. The value of specific heat c_p is 1.24 Btu/(lb)($^\circ$R) and is constant, the ratio of specific heats γ is 1.667, and the gas constant R is 386 ft-lb/(lb)($^\circ$R).

Friction Coefficients

Friction data were obtained both with and without heat transfer. The average friction coefficient was calculated from the experimental pressure drop data as follows: The friction pressure drop Δp_{fr} was obtained by subtracting the calculated momentum pressure drop Δp_{mom} from the measured static-pressure drop, across the test section. Thus,

$$\Delta p_{fr} = \Delta p - \Delta p_{mom} = \Delta p - \frac{G^2 R}{g}\left(\frac{t_2}{p_2} - \frac{t_1}{p_1}\right) \tag{1}$$

where t_1 and t_2 are the absolute static temperatures at the entrance and exit of the test sections, respectively. In general, the static temperatures were calculated from the measured values of gas flow, static pressure, and the total temperature by the following equation, which is obtained by combining the perfect gas law, the equation of continuity, and the energy equation:

$$t = -\frac{\gamma g}{(\gamma-1)R}\left(\frac{p}{G}\right)^2 + \sqrt{\left[\frac{\gamma g}{(\gamma-1)R}\left(\frac{p}{G}\right)^2\right]^2 + 2T\frac{\gamma g}{(\gamma-1)R}\left(\frac{p}{G}\right)^2} \tag{2}$$

For the bellmouth entrance the static temperature t_1 could be represented by the relation

$$t_1 = T_1 \left(\frac{p_1}{P_1}\right)^{\frac{\gamma-1}{\gamma}} \tag{3}$$

In equation (3) the total pressure at the test-section entrance P_1 was assumed to be equal to the static pressure in the entrance mixing tank, where the velocity was negligible.

The average friction coefficient was calculated from the relation

$$f = \frac{\Delta p_{fr}}{4\frac{L}{D}\frac{\rho_{av}V^2}{2g}} = \frac{g\rho_{av}\Delta p_{fr}}{2\frac{L}{D}G^2} \tag{4}$$

where the density ρ_{av} was evaluated at the average static pressure and temperature of the gas as follows:

$$\rho_{av} = \frac{1}{R}\left(\frac{p_1 + p_2}{t_1 + t_2}\right) \tag{5}$$

The average friction coefficient was also calculated with the density evaluated at the film temperature as shown in the following equation:

$$f_f = \frac{\Delta p_{fr}}{4\frac{L}{D}\frac{\rho_f V^2}{2g}} = \left(\frac{\rho_{av}}{\rho_f}\right)f = \left(\frac{2T_f}{t_1 + t_2}\right)f \tag{6}$$

The friction coefficients will be discussed in the following section.

Heat-Transfer Coefficient

The average heat-transfer coefficient h_{av} was computed from the experimental data by the relation

$$h_{av} = \frac{Q}{S(T_s - T_b)} \tag{7}$$

where

$$Q = Wc_{p,b}(T_2 - T_1) \tag{8}$$

and the average surface temperature T_s was taken as an integrated average of the local outside wall temperature minus the temperature drop through the wall. The temperature of the gas T_b was taken as the arithmetic mean of the total temperatures at the entrance T_1 and the exit T_2 of the test section.

The average heat-transfer coefficient was used to calculate the Nusselt number using the following relation

$$Nu_{av} = h_{av}D/k \tag{9}$$

where h_{av} is the average heat-transfer coefficient, D the inside diameter of the test section, and k the thermal conductivity of the gas. The Nusselt number was calculated with thermal conductivities evaluated at surface, bulk, and film temperatures.

The heat loss to the surroundings was calculated by the following equation:

$$Q_L = Q_E - Q \tag{10}$$

where Q_E is the rate of electric heat input and Q is the rate of heat transfer to the gas. For most runs more than 80 percent of the heat generated was transferred to the gas. It was possible to calculate local heat-transfer coefficients by evaluating the various local heat losses and then making a heat balance. The heat losses were calculated as follows:

(1) The heat loss at the ends of the test section by conduction was calculated using the following equation:

$$Q_c = k_t A \frac{dT}{dL} \tag{11}$$

where dT/dL is the slope of the axial wall temperature distribution at the entrance and exit of the test section, k_t is the thermal conductivity of the tube material and A is the cross-sectional area of the tube.

(2) Local radial heat loss through the insulation for each increment of length ΔL was calculated using the following equation:

$$Q_{\Delta L} = k_z \frac{2\pi\Delta L}{\ln \frac{r_o}{r_i}} (T_{zi} - T_{zo}) \tag{12}$$

where T_{zi} and T_{zo} are inside and outside wall temperatures, respectively, of the insulating cylinder, k_z is the thermal conductivity of the insulation evaluated at the average insulation temperature, and r_i and r_o are the inside and outside radii, respectively, of the insulating cylinder.

(3) The sum of the local radial heat losses and the end losses was found to account for more than 80 percent of the total heat loss calculated by equation (10). Each local heat loss and the end losses were increased by the ratio of total heat loss to the sum of local heat losses.

(4) The rate of heat conduction into and away from each increment, $Q_{c,in}$ and $Q_{c,out}$, respectively, was calculated using equation (11) and taking dT/dL as the slope of the axial temperature distribution at the ends of the increment being calculated.

(5) The rate of electrical heat generation in each increment Q_e was calculated by multiplying the current through the test section by the voltage drop across the increment.

(6) A heat balance was then set up for each increment starting at the entrance, as follows:

$$Q_e + Q_{c,in} - Q_{c,out} - Q_{\Delta L} - Q = 0 \qquad (13)$$

from which it was possible to calculate the rate of heat transfer to the gas Q from each increment. The bulk temperature of the gas leaving each increment could be calculated by using the equation

$$Q = Wc_{pb} (T_{out} - T_{in}) \qquad (14)$$

where T_{in} is the bulk temperature of the gas entering the increment and T_{out} is the bulk temperature of the gas leaving the increment. This was repeated for each succeeding increment and the outlet gas temperature was compared with the measured outlet gas temperature (station 2) as a check on the computation.

(7) The local bulk temperature and local surface temperature along with the heat-transfer area for the increment and the rate of heat transfer to the gas for the increment were used to calculate a local heat-transfer coefficient using the same type of equation used to calculate the average heat-transfer coefficient. Nusselt number based on the local heat-transfer coefficient was calculated and will be discussed along with the average Nusselt number in the following section.

RESULTS AND DISCUSSION

Axial Wall Temperature Distributions

In figure 5 representative axial outside wall temperatures are shown for a tungsten tube with a length-to-diameter ratio of 92. The outside

wall temperature is plotted against dimensionless distance x/L for three different average wall temperatures. The rate of heat transfer to the gas, the mass flow, the average inside wall temperature, the temperature rise of the gas, and the thermocouple and optical pyrometer temperature measurements are tabulated in figure 5.

The increase in the slope of each axial wall temperature distribution is probably due to the increase in resistivity with temperature (the resistivity at 4000° R is twice that at 2000° R). The large axial temperature gradients at the entrance and exit of the test section are the result of conduction losses to the connecting flanges, mixing tanks, and electrical connectors.

Friction Coefficients

The average friction coefficient for both the adiabatic and heated runs is shown in figures 6 and 7. The line representing the Kármán-Nikuradse relation between friction coefficient and Reynolds number for turbulent flow

$$\frac{1}{\sqrt{\frac{8f}{2}}} = 2 \log \left(\frac{GD}{\mu} \sqrt{8 \frac{f}{2}} \right) - 0.8 \qquad (15)$$

and the laminar flow line

$$\frac{f}{2} = \frac{8}{\frac{GD}{\mu}} \qquad (16)$$

are included in figures 6 and 7 for comparison.

For Reynolds numbers above 6000, the average friction coefficients for adiabatic flow are in very good agreement with the turbulent flow

line. In the lower Reynolds number region the coefficients drop off and approach the laminar flow line as would be expected in the transition region. The extension of the transition region to a Reynolds number of 6000 was due to the effect of the bellmouth entrance. The average friction coefficients with the density evaluated at bulk temperature (eq. 5) are shown in figure 6. The data from the present investigation are in fair agreement with the predicted line for the higher Reynolds number range.

References 1 and 6 indicate that average friction coefficients are best correlated with density evaluated at the film temperature and using a modified Reynolds number based on film temperature. Data from the present investigation are shown evaluated in this manner in figure 7. The friction coefficients fall somewhat higher than the Kármán-Nikuradse line but good agreement exists with the data of references 1 and 6.

Heat-Transfer Coefficients

The results of reference 1 indicate that the average Nusselt number for various ratios of surface-to-bulk temperature and length to diameter are best represented by the following:

$$\frac{h_{av}D}{k_f} = 0.034\left(\frac{\rho_f VD}{\mu_f}\right)^{0.8}\left(\frac{c_{pf}\mu_f}{k_f}\right)^{0.4}\left(\frac{L}{D}\right)^{-0.1} \tag{17}$$

where all the physical properties and the density are evaluated at the film temperature and the modified Reynolds number is used.

An alternate method of correcting for the effect of the length-to-diameter ratio is the use of the following equation:

$$\frac{h_{av}D}{k_f} = 0.021\left(\frac{\rho_f VD}{\mu_f}\right)^{0.8}\left(\frac{c_{pf}\mu_f}{k_f}\right)^{0.4}\left(1 + \left[\frac{L}{D}\right]^{-0.7}\right) \qquad (18)$$

where the use of $1 + \frac{L}{D}^{-0.7}$ in place of $\frac{L}{D}^{-0.1}$ and the corresponding difference in constants makes the relation more general since it is applicable to all length-to-diameter ratios. The data of the present investigation with the properties evaluated at the film temperature are shown in figure 8 as a function of modified Reynolds number. For Reynolds numbers less than 10,000 the present data are in poor agreement with equation (18). Above a Reynolds number of 10,000 the data agree to within 10 percent.

For the limited range of Reynolds number in this investigation the average heat-transfer data seem to be correlated better by evaluating the physical properties and density at the surface temperature. The results are shown in figure 9.

Since there could be some question as to the significance of average heat-transfer coefficients when the heat flux varies as much as is indicated by the axial wall temperature distributions shown in figure 5, it seemed desirable to calculate local heat-transfer coefficients. Ratios of local surface temperature to local bulk temperatures were considerably higher than ratios of the averages of these temperatures. Local heat-transfer data are shown in figure 10 where the film Nusselt number is plotted as a function of modified Reynolds number. The data are in fair agreement with the line obtained by McAdams (ref. 7) from correlation of the results of various investigators. The equation corresponding to this reference line is

$$\frac{hD}{k_f} = 0.023\left(\frac{\rho_f VD}{\mu_f}\right)^{0.8}\left(\frac{c_{pf}\mu_f}{k_f}\right)^{0.4} \qquad (19)$$

The same data, shown in figure 11 with the physical properties and density evaluated at the surface temperature, fall higher than the predicted line. However, the spread of the data is decreased from about 38 percent in figure 10 to about 25 percent in figure 11. Heat-transfer coefficients for the first two increments and the last increment were not used because of entrance effects and the large end losses.

SUMMARY OF RESULTS

The following summary gives the results of this investigation of heat transfer and pressure drop for helium flowing through electrically heated smooth tubes with length-to-diameter ratios of 60 and 92 for the following range of conditions: average surface temperature from 1457° to 4533° R, Reynolds number from 3150 to 60,000, heat flux up to 345,000 Btu per hour per square foot of heat transfer area and exit Mach number to 1.0:

1. In general, the correlation of both local and average heat-transfer coefficients is in agreement with that of previous investigations of average heat-transfer coefficients at lower surface temperatures and heat flux. The physical properties and density used in the Nusselt, Prandtl, and Reynolds numbers were evaluated at the film temperature that is midway between the surface and bulk temperatures, a modified Reynolds number was used, and a correction for length-to-diameter ratio was applied. For low Reynolds numbers better correlation results if the physical properties and density are evaluated at the surface temperature.

2. Friction coefficients with no heat transfer are in good agreement with those obtained by other investigators. The friction coefficients obtained with heat addition are in fair agreement with the Kármán-Nikuradse line when the average density is evaluated at the gas temperature. Evaluation of the density at the film temperature, as done in previous investigations, gave rather poor agreement with the accepted line.

APPENDIX - METHOD OF OPTICAL PYROMETRY

As mentioned in a previous section, the temperatures above approximately 3200° F were measured with an optical pyrometer. Since the insulated test section did not approximate a blackbody, it was necessary to correct the temperature readings of the pyrometer.

A relation between the true temperature of an object and the brightness temperature indicated by the optical pyrometer can be obtained from Weins' formula for blackbody radiation

$$J_{bb} = C_1 \lambda^{-5} e^{-C_2/\lambda T_{bb}} \tag{A1}$$

where J_{bb} is the rate of emission of radiant energy at wavelength λ from a blackbody at temperature T_{bb}, and C_1 and C_2 are known constants. The same formula can be applied to a nonblackbody at true temperature T_{bb}, and can be written

$$J_{br} = \epsilon_\lambda C_1 \lambda^{-5} e^{-C_2/\lambda T_{bb}} = C_1 \lambda^{-5} e^{-C_2/\lambda T_{br}} \tag{A2}$$

where T_{br} is the brightness temperature.

The ratio of J_{br} to J_{bb} is defined as the spectral emissivity ϵ_λ of the nonblackbody under consideration, as follows:

$$\epsilon_\lambda = \frac{J_{br}}{J_{bb}} = \frac{C_1 \lambda^{-5} e^{-C_2/\lambda T_{br}}}{C_1 \lambda^{-5} e^{-C_2/\lambda T_{bb}}} \tag{A3}$$

therefore,

$$\ln \epsilon_\lambda = -\frac{C_2}{\lambda T_{br}} + \frac{C_2}{\lambda T_{bb}} = \frac{C_2}{\lambda}\left[\frac{1}{T_{bb}} - \frac{1}{T_{br}}\right] \tag{A4}$$

The interposition of a view window between the heated object and the optical pyrometer, necessitates a modification of equation (A4) to include the spectral transmissivity τ of the window. The spectral transmissivity is defined as the ratio of the transmitted radiant energy to the incident radiant energy for a given wavelength as shown,

$$\tau_\lambda = \frac{J_\tau}{J_{br}} = \frac{C_1\lambda^{-5} e^{-C_2/\lambda T_\tau}}{C_1\lambda^{-5} e^{-C_2/\lambda T_{br}}} \tag{A5}$$

where T_τ is the temperature of a heated body measured with the optical pyrometer with the window interposed, and T_{br} is the optical pyrometer brightness temperature measured under the same conditions with the exception that no window is interposed. Both measurements would be made while the blackbody temperature remained constant. Equation (A5) can also be expressed as

$$\ln \tau_\lambda = \frac{C_2}{\lambda}\left[\frac{1}{T_{br}} - \frac{1}{T_\tau}\right] \tag{A6}$$

solving equation (A6) for T_{br} gives

$$T_{br} = \frac{C_2/\lambda}{\ln \tau_\lambda + \frac{C_2}{\lambda T_\tau}} \tag{A7}$$

and substituting this expression for T_{br} into equation (A4) gives

$$\ln(\epsilon_\lambda \tau_\lambda) = \frac{C_2}{\lambda}\left[\frac{1}{T_{bb}} - \frac{1}{T_\tau}\right] \tag{A8}$$

which can be written

$$T_{bb} = \frac{C_2/\lambda}{\ln(\epsilon_\lambda \tau_\lambda) + \frac{C_2}{\lambda T_\tau}} \tag{A9}$$

This expression can be used to calculate the actual temperature of a heated body by measuring the temperature T_τ with an optical pyrometer if the spectral emissivity of the heated body ϵ_λ and the transmissivity of the window τ_λ are known.

The transmissivity of a view window can be determined very easily experimentally by measuring the temperature of a calibration lamp both with and without the window interposed and by inserting these values into equation (A6).

There are values of spectral emissivity for tungsten and molybdenum in the literature but these values are for flat polished specimens with all radiation originating from the specimen. These conditions are not very closely approximated by most heat-transfer test sections; that is, the test sections used in the present investigation were circular tubes whose surfaces did not remain polished because of grain growth and a small amount of oxidation; some of the radiation incident to the optical pyrometer was emitted and reflected from the hot radiation shield. As a matter of fact it is more correct to say that it is the effective spectral emissivity in which we are now interested. The method of determining this effective emissivity was to measure the temperature of the test section with an optical pyrometer and thermocouple simultaneously, insert them

into equation (A8) resulting in a value for $\ln(\epsilon_\lambda \tau_\lambda)$, which could be used to compute ϵ_λ since τ_λ had been previously determined. The values of ϵ_λ could be plotted as a function of temperature up to the point where the thermocouples failed (about 3200° F) and then extrapolated to the higher temperatures. With these values of ϵ_λ and τ_λ, equation (A9) could be used to determine the true wall temperature with the optical pyrometer.

The values for effective spectral emissivity might have been in error, especially in the extrapolated region. The effect of an error in emissivity on the test section wall temperature calculated by equation (A9) is tabulated below:

Measured temperature, T_τ °F	Effective spectral emissivity, $\epsilon_\lambda \tau_\lambda$	Calculated true temperature, T_{bb} °F
5000	0.5	5570
5000	.6	5410
5000	.7	5280

From this table it can be seen that fairly large errors in effective spectral emissivity do not seem to affect the wall temperatures appreciably.

REFERENCES

1. Humble, Leroy W., Lowdermilk, Warren H., and Desmon, Leland G.: Measurements of Average Heat-Transfer and Friction Coefficients for Subsonic Flow of Air in Smooth Tubes at High Surface and Fluid Temperatures. NACA Rep. 1020, 1951. (Supersedes NACA RM's E7L31, E8L03, E50E23, and E50H23.)

2. Durham, F. P., Neal, R. C., and Newman, H. J.: High Temperature Heat Transfer to a Gas Flowing in Heat Generating Tubes with High Heat Flux. TID-7529, P. 1, book 2, Reactor Heat Transfer Conf., Nov. 1957, pp. 502-514.

3. Woolley, Harold W.: Helium. Table 6.10 of the NBS-NACA Tables of Thermal Properties of Gases, NBS, 1950.

4. Nuttall, R. L.: Helium, Table 6.39 of the NBS-NACA Tables of Thermal Properties of Gases, NBS, 1950.

5. Nuttall, R. L.: Helium, Table 6.42 of the NBS-NACA Tables of Thermal Properties of Gases, NBS, 1950.

6. Weiland, Walter F., and Lowdermilk, Warren H.: Measurements of Heat-Transfer and Friction Coefficients for Air Flowing in a Tube of Length-Diameter Ratio of 15 at High Surface Temperatures. NACA RM E53E04, 1953.

7. McAdams, William H.: Heat Transmission. Third ed., McGraw-Hill Book Co., Inc., 1954.

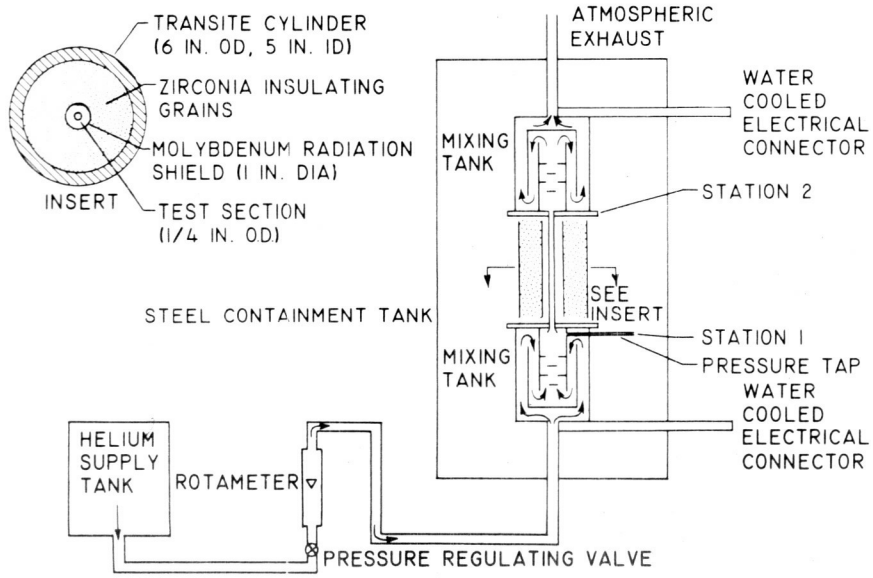

Fig. 1. - Schematic diagram showing arrangement of test apparatus.

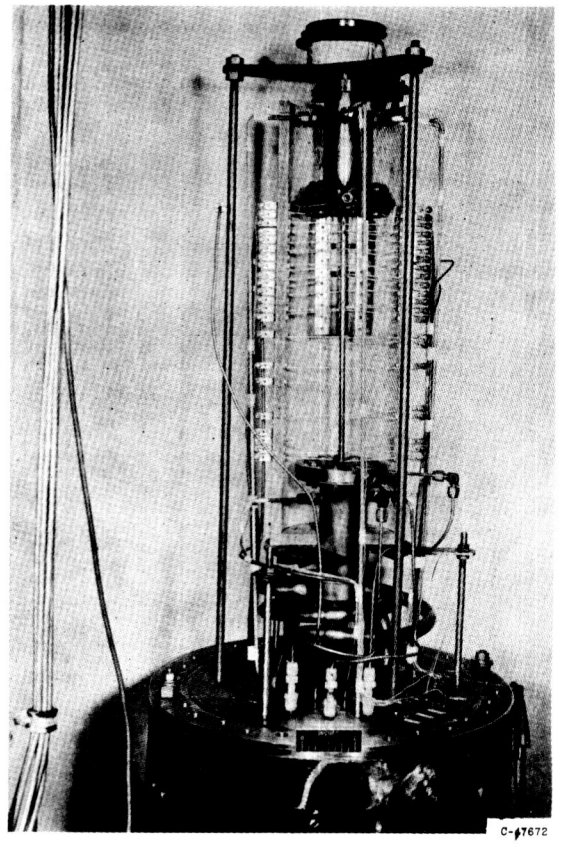

Fig. 2. - High-temperature heat-transfer apparatus.

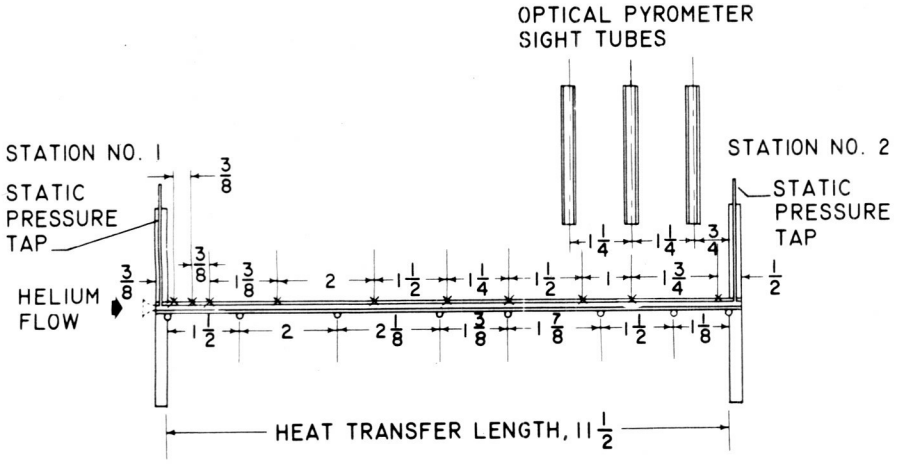

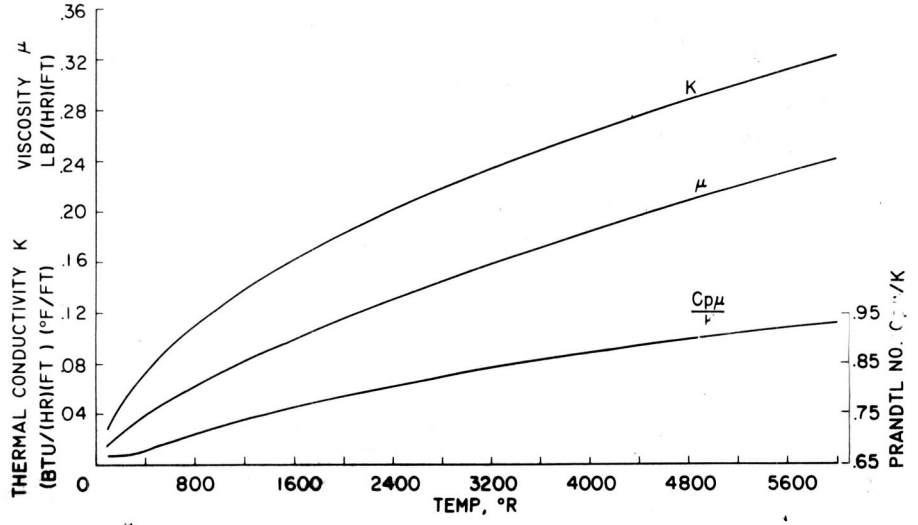

Fig. 4. - Variation of thermal conductivity, absolute viscosity, and Prandtl number of helium with temperature.

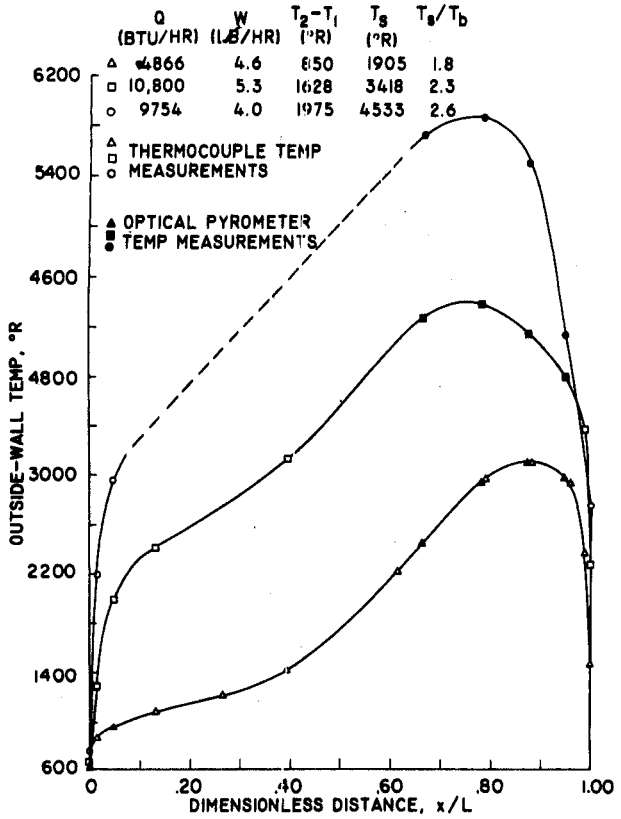

Fig. 5. - Representative outside-wall temperature distribution for various amounts of heat input to air. Tungsten tube, length-diameter ratio, 92.

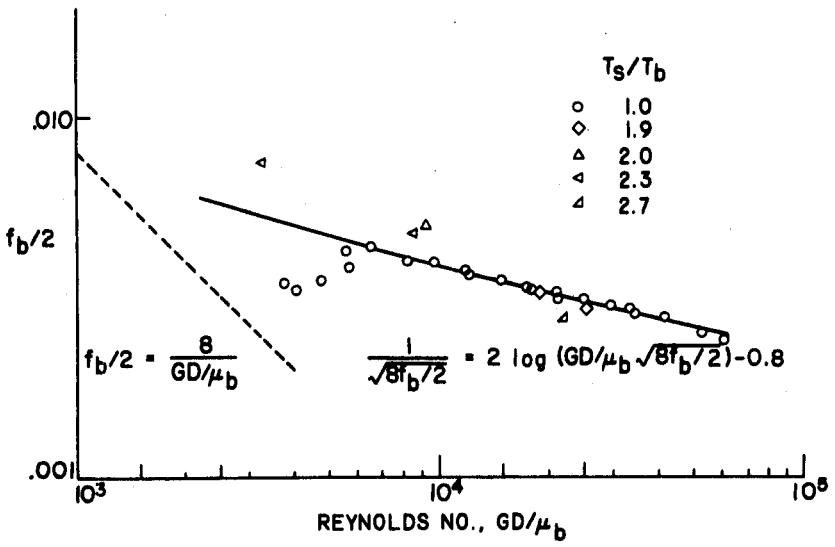

Fig. 6. - Correlation of average friction coefficients. Viscosity and density evaluated at bulk temperature, T_b.

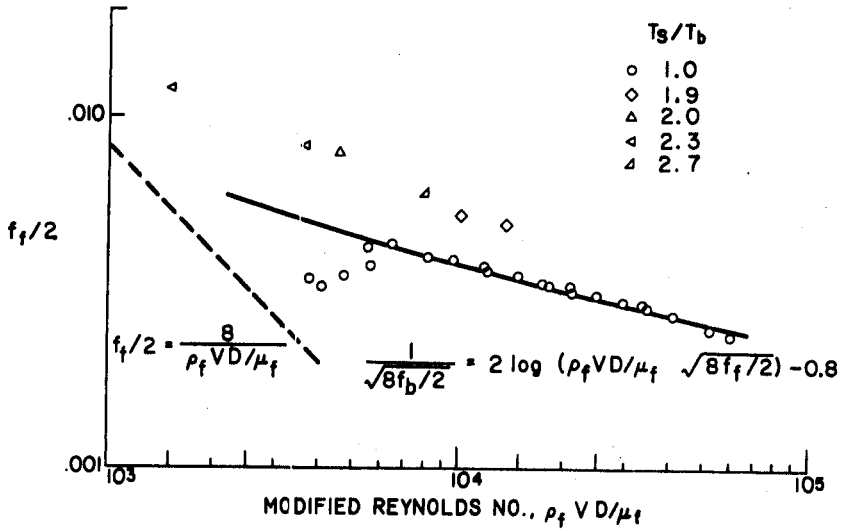

Fig. 7. - Correlation of average friction coefficients. Viscosity and density evaluated at film temperature, T_f.

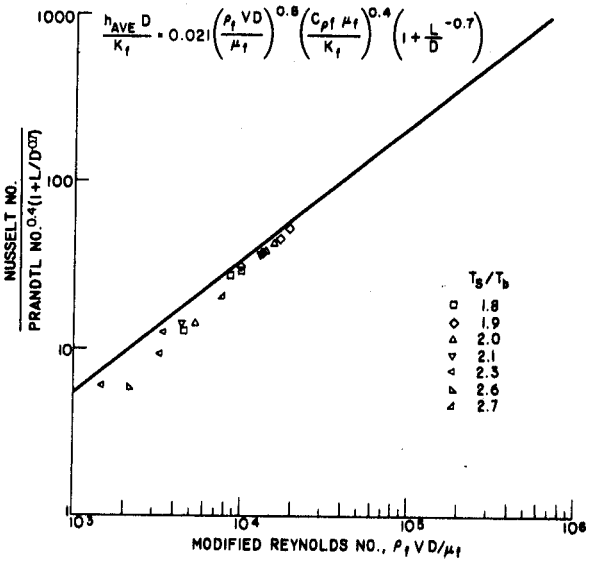

Fig. 8. - Correlation of average heat-transfer coefficients with variable heat flux. Length-diameter ratios of 80 and 92; properties of helium evaluated at film temperature, T_f.

TAYLOR

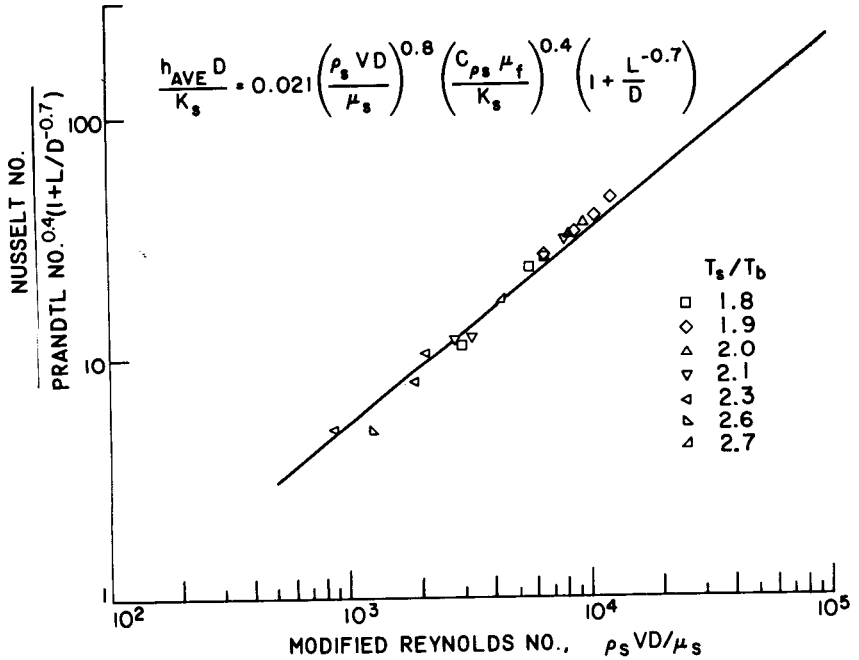

Fig. 9. - Correlation of average heat-transfer coefficients with variable heat flux. Length-diameter ratios of 60 and 92; properties of helium evaluated at surface temperature, T_s.

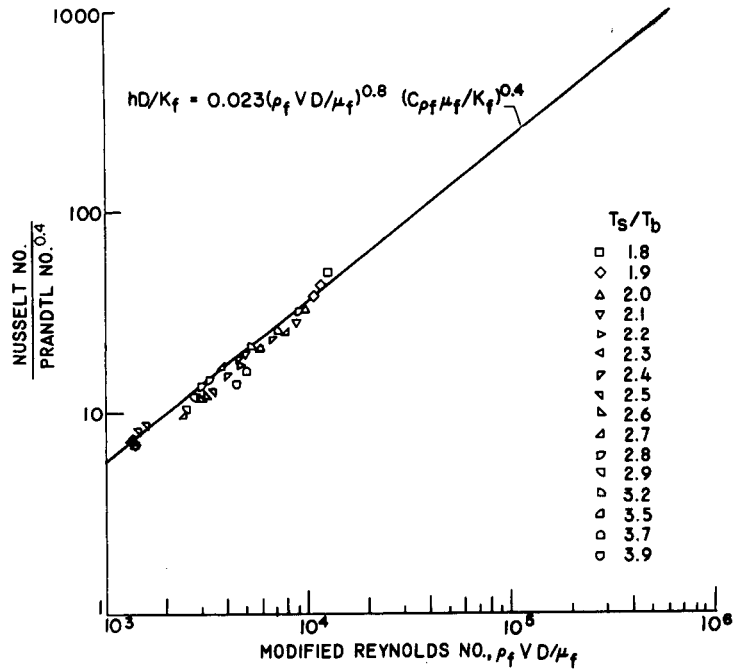

Fig. 10. - Correlation of local heat-transfer coefficients with variable heat flux. Over-all length-diameter ratio, 60; bellmouth entrance; properties of helium evaluated at film temperature, T_f.

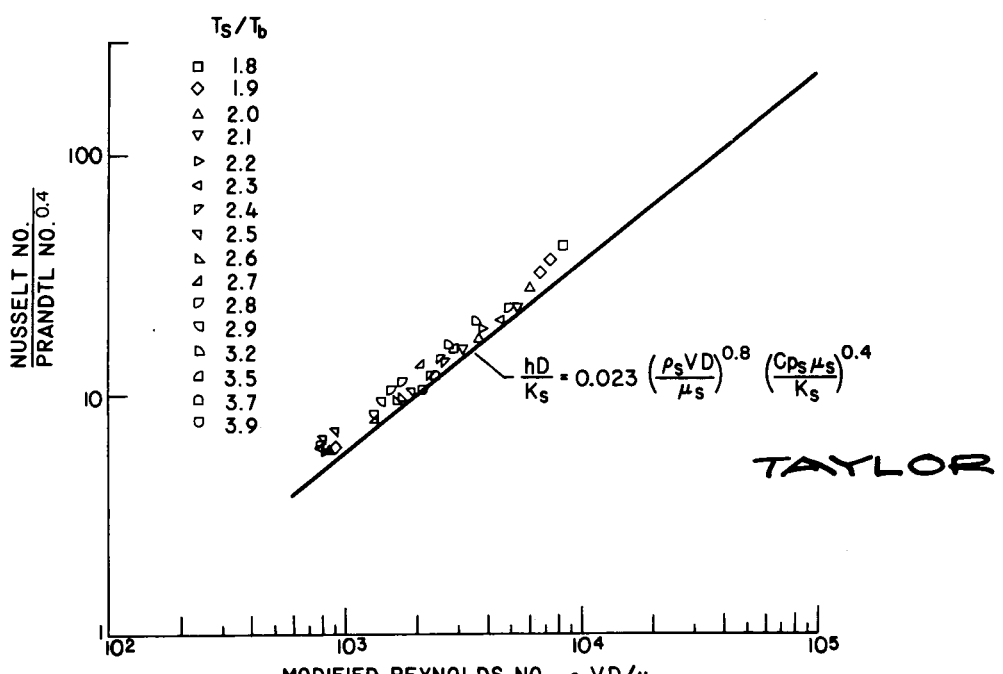

Fig. 11. - Correlation of local heat-transfer coefficients with variable heat flux. Over-all length-diameter ratio, 60; bellmouth entrance; properties of helium evaluated at surface temperature, T_s.